

# Earth's Future

## RESEARCH ARTICLE

10.1029/2024EF004716

### Key Points:

- This study presents a flexible approach to the challenge of selecting climate projections for decision-making
- We find projected temperature and precipitation changes will stress groundwater resources in the Edwards Aquifer using this approach

### Supporting Information:

Supporting Information may be found in the online version of this article.

### Correspondence to:

A. M. Wootten,  
amwoote@ou.edu

### Citation:

Wootten, A. M., Başağaoğlu, H., Bertetti, F. P., Chakraborty, D., Sharma, C., Samimi, M., & Mirchi, A. (2024). Customized statistically downscaled CMIP5 and CMIP6 projections: Application in the Edwards aquifer region in south-central Texas. *Earth's Future*, 12, e2024EF004716. <https://doi.org/10.1029/2024EF004716>

Received 9 APR 2024  
Accepted 21 AUG 2024

© 2024. The Author(s).

This is an open access article under the terms of the [Creative Commons Attribution License](#), which permits use, distribution and reproduction in any medium, provided the original work is properly cited.

# Customized Statistically Downscaled CMIP5 and CMIP6 Projections: Application in the Edwards Aquifer Region in South-Central Texas

A. M. Wootten<sup>1</sup> , H. Başağaoğlu<sup>2</sup>, F. P. Bertetti<sup>2</sup> , D. Chakraborty<sup>3</sup>, C. Sharma<sup>3</sup>, M. Samimi<sup>2</sup>, and A. Mirchi<sup>4</sup> 

<sup>1</sup>South Central Climate Adaptation Science Center, University of Oklahoma, Norman, OK, USA, <sup>2</sup>Edwards Aquifer Authority, San Antonio, TX, USA, <sup>3</sup>School of Civil and Environmental Engineering, and Construction Management, University of Texas at San Antonio, San Antonio, TX, USA, <sup>4</sup>Department of Biosystems and Agricultural Engineering, Oklahoma State University, Stillwater, OK, USA

**Abstract** Climate projections are being used for decision-making related to climate mitigation and adaptation and as inputs for impacts modeling related to climate change. The plethora of available projections presents end users with the challenge of how to select climate projections, known as the “practitioner’s dilemma.” In addition, if an end-user determines that existing projections cannot be used, then they face the additional challenge of producing climate projections for their region that are useful for their needs. We present a methodology with novel features to address the “practitioner’s dilemma” for generating downscaled climate projections for specific applications. We use the Edwards Aquifer region (EAR) in south-central Texas to demonstrate a process to select a subset of global climate models from both the CMIP5 and CMIP6 ensembles, followed by downscaling and verification of the accuracy of downscaled data against historical data. The results show that average precipitation changes range from a decrease of 10.4 mm to an increase of 25.6 mm, average temperature increases from 2.0°C to 4.3°C, and the number of days exceeding 37.8°C (100°F) increase by 35–70 days annually by the end of century. The findings enhance our understanding of the potential impacts of climate change on the EAR, essential for developing effective regional management strategies. Additionally, the results provide valuable scenario-based projected data to be used for groundwater and spring flow modeling and present a clearly documented example addressing the “practitioner’s dilemma” in the EAR.

**Plain Language Summary** Groundwater, constituting over one-third of global water resources, is crucial for sustaining ecosystems, agriculture, and drinking water supplies. In the face of climate change, rising temperatures and shifting precipitation patterns are anticipated to diminish the availability of groundwater for both societal and ecological requirements. Regional managers, in preparing for these changes, need localized climate projections for effective planning. However, the abundance of available climate projections poses a significant challenge for decision-makers in climate adaptation, known as the “practitioner’s dilemma.” This dilemma, though widely acknowledged, lacks a standardized solution. Our paper introduces a methodology to navigate this challenge, specifically tailored to the needs of the Edwards Aquifer Authority. This authority is actively engaged in implementing protection and habitat conservation plans to alleviate stress on groundwater and major springs in the Edwards Aquifer Region, located in south-central Texas. Our projections indicate that rising temperatures are likely to increase evapotranspiration, thereby exacerbating the strain on groundwater resources in this region as climate conditions evolve. Furthermore, our approach offers a customizable approach to “the practitioner’s dilemma,” potentially serving as a model for other decision-makers in the United States to effectively utilize climate projections in their strategic planning.

## 1. Introduction

More than one-third of global water supplies emanate from groundwater (Famiglietti, 2014), which is indispensable for human health, ecosystems, and energy and food security (Giordano, 2009). Groundwater plays a critical role in meeting consumptive water use needs and sustaining ecology, especially when surface water resources are scarce. Nearly 70% of groundwater withdrawals have been allocated to sustain agricultural production worldwide (Margat & Gun, 2013; Rosegrant et al., 2009). In the United States, groundwater provides about 40% of water for agriculture and domestic supplies (Lall et al., 2018; Russo & Lall, 2017). The intensive use of groundwater, particularly for irrigation, has caused groundwater overdraft in some regions when withdrawal

rates exceeded recharge rates (Ferguson & Gleeson, 2012; Loáiciga, 2009; McCabe & Wolock, 2016; Siebert et al., 2010). Additional stressors may include higher pumping rates driven by population growth and socio-economic developments that could exacerbate groundwater depletion (Costantini et al., 2023; Shaabani et al., 2023; Wu et al., 2020). Elevated temperatures and shifts in precipitation patterns resulting from climate change could increase evapotranspiration and affect availability of recharge, leading to greater depletion of groundwater in some groundwater basins (Condon et al., 2020). Conversely, these changes could result in increased flooding and added recharge in other groundwater basins (Costantini et al., 2023). Thus, region-specific climate change assessments are needed to effectively manage future groundwater sustainability.

At global and continental scales, most climate projections use output from global climate models (GCMs). However, regional and local climates are not well represented by GCMs due to their coarse resolution ( $\geq 100$  km, Rummukainen, 2010). Statistical downscaling techniques can translate the climate response simulated by GCMs to smaller spatial scales, reducing biases and adding information for decision makers (Rummukainen, 2016; Tabari et al., 2016). In addition, the use of statistical downscaling has allowed for GCM projections to be incorporated in impact assessment analyses. These assessments include studies that examined impacts to groundwater and aquifers (e.g., Gordu & Nachabe, 2023; Scibek & Allen, 2006), streamflow (e.g., Neves et al., 2020; Wootten et al., 2023), aquatic ecosystems and species (e.g., Keller et al., 2022), and water resources, quality, and security (Bhatt et al., 2023; Fu et al., 2022; Jaramillo & Nazemi, 2018). In a recent study, Chakraborty et al. (2021) assessed the impacts of potential future climates on groundwater levels in the Edwards Aquifer using MACA downscaled projected climatic data from CMIP5. However, MACA-downscaled data sets were developed for much larger areas of the United States at coarser spatial resolution, which presents a challenge in accurately representing regional climatic characteristics (Lall et al., 2018).

The “practitioner's dilemma” is not the lack of available data and projections, but the challenge of choosing and using projections wisely in regional decision making (Barsugli et al., 2013) and each of the aforementioned studies grappled with this challenge. While the “practitioner's dilemma” is a well-recognized challenge to using downscaled climate projections, there are no standard practices defined to handle that challenge, though there are studies building toward that standardization (e.g., Jagannathan et al., 2020, 2021, 2023; Maraun, 2023). The “practitioner's dilemma” traditionally focuses on selecting from pre-existing data sets but not on the case when new projections are needed, and pre-existing projections do not meet those needs. This study contributes to addressing the “practitioner's dilemma” through a presented approach to selecting GCMs and downscaling them for the Edwards Aquifer Region (EAR).

The Edwards Aquifer in south central Texas is a karst aquifer that is the primary drinking water source for more than 2 million people and provides important environmental flows, sustaining habitats for several threatened/endangered species at two major spring systems. The sustainability of the Edwards Aquifer depends on a delicate balance between recharge, withdrawals, spring flow, and runoff, all of which can be affected by climate change. Several studies have examined historical and projected future climate effects on the sustainability of water resources in south central Texas. Using earlier generations of GCMs, Loáiciga et al. (2000) noted that without considering variations in aquifer recharge and the implementation of sound pumping strategies, the water resources of the Edwards Aquifer could be severely impacted under future warmer climates. Based on projected temperature increases and projected decreases in spring flow for the region, Devitt et al. (2019) concluded that groundwater-bound species in the Edwards Aquifer system are at a high risk of extinction within the next century. Using projected climate data sets for the Edwards Aquifer region, statistically downscaled from CMIP5 models using the Multivariate Adaptive Constructed Analogs (MACA, Abatzoglou & Brown, 2012), Chakraborty et al. (2021) concluded that the combined effects of increased evapotranspiration, decreased soil moisture, and reduced diffuse recharge due to projected higher future temperatures could intensify hydrological droughts and reduce groundwater levels, exacerbating groundwater sustainability challenges. The Edwards Aquifer Authority (EAA) has been implementing several aquifer protection programs to support established habitat conservation plans and to mitigate stress on the groundwater and major springs that provide habitat for threatened and endangered species (Committee to Review the Edwards Aquifer Habitat Conservation Plan, Phase 3 et al., 2018). Accurate assessment of the effectiveness of these protection programs under future climate conditions and regional socioeconomic developments depends on the careful selection and creation of climate projections, which reflects the EAA's own “practitioner's dilemma”.

Typically, the “practitioner's dilemma” pertains to selecting from existing downscaled climate projections. However, an added layer of the “practitioner's dilemma” arises when existing projections do not meet user needs. In such cases, developing new projections becomes necessary, as exemplified by the requirements of the EAA. However, this secondary challenge is often overlooked in the literature and was not addressed by Barsugli et al. (2013). We note the reasons for creating fine resolution (~1 km) projections in this study rather than relying on other data sets such as the CMIP6-LOCA2 (Pierce et al., 2023) or the CMIP6-STAR (Hayhoe et al., 2023), contributing to the literature regarding the choice between utilizing existing data versus creating new data sets. The groundwater flow models developed and used by the EAA to simulate and forecast groundwater levels and spring flow under current and projected climate conditions rely on gridded data at a spatial resolution of 0.4 km. Such fine resolution is critical for accurately capturing spatiotemporal variations in mean and extreme climate events and their combined effects with spatial variations in hydrogeologic and topographic features (Figure S1a in Supporting Information S1) on aquifer recharge and regional groundwater flow patterns. Specifically, the fine-resolution representation of areas with heavy storms and extreme precipitation events along ephemeral and perennial streams is crucial because extreme precipitation-driven focused recharge along discrete features (e.g., sinkholes) and dissolution along faults and fractures within stream channels are more significant for aquifer recharge than gravity-driven dispersed recharge over inter-stream areas in the EAR (Sun et al., 2020). Raw GCM data are unable to capture these features (Figure S1b in Supporting Information S1). Other downscaled projections, including CMIP6-LOCA2 and CMIP6-STAR in the literature, have a resolution from 4 to 6 km, which also does not capture these critical features (Figure S1c in Supporting Information S1). Therefore, custom downscaling to 1 km was deemed necessary for this project and successfully captured the topographic effects in the EAR (Figure S1d in Supporting Information S1). The decision to create custom 1 km projections aligns with previous literature suggesting that a spatial resolution finer than 4 km is required to accurately assess climate impacts on vegetation dynamics in complex topography (e.g., Franklin et al., 2013).

This study presents an approach to addressing the “practitioner's dilemma” for the EAA as our contribution to the larger discussion regarding the development and use of decision-relevant climate projections. In addition, this study generates customized downscaled climate projections for the Edwards Aquifer Region (hereafter EAR) of south-central Texas to facilitate the assessment of the potential impacts of climate change on groundwater levels and spring flows. The fine resolution (~1 km) downscaled projections are specifically designed to capture the historical climate of the region and account for multiple known sources of uncertainty in the climate projections (Crosbie et al., 2011; Lafferty & Sriver, 2023; Wootten et al., 2017). The following sections describe the approach to GCM selection and downscaling and the insights for future impacts modeling efforts, essential for evaluating the long-term sustainability of the EAR amid a changing climate.

## 2. Region, Data, and Methods

### 2.1. Study Region

The Edwards Aquifer is characterized by faulted and fractured carbonate rocks, heterogeneous hydrogeological properties and flow pathways, conduit flow, presence of sinkholes, sinking streams, caves, ecologically rich springs, and highly productive water wells. The San Antonio segment of the Edwards Aquifer system covers an area of approximately 14,200 km<sup>2</sup> (5,490 mi<sup>2</sup>) and is divided into three distinct hydrogeological zones from north to south, including the contributing zone, recharge zone, and the artesian zone, as shown in Figure 1 (Lindgren et al., 2004; Schindel, 2019). Spring flow and runoff in the contributing zone feed streams that cross the outcrop of the Edwards Limestone in the recharge zone. Faulting (Balcones Faut Zone), fractures, and karst features facilitate vertical downward percolation of surface water, recharging the aquifer. The artesian zone of the aquifer, where most of the large production wells are located, is confined and fully saturated. The Edwards Aquifer is the primary water source for much of the area, including the City of San Antonio and surrounding communities. The aquifer also provides habitat for several threatened and endangered groundwater-bound endemic species such as the Texas blind salamander and Fountain darter (Committee to Review the Edwards Aquifer Habitat Conservation Plan, Phase 3, 2018) at the major springs in the region, including Comal Springs and San Marcos Springs. The EAR is in the southern tip of the Southern Great Plains (SGP) region of the United States and has a distinct precipitation gradient from east to west (Figure 1). The domain for the downscaling covers the EAR from 28.75°N to 30.50°N and 100.75°W to 97.75°W. The entire SGP region is used for the evaluation and ensemble subset selection of the GCMs, as GCMs are more capable of representing physical processes on the scale of the SGP region and the continental United States than in the relatively smaller domain of the EAR.

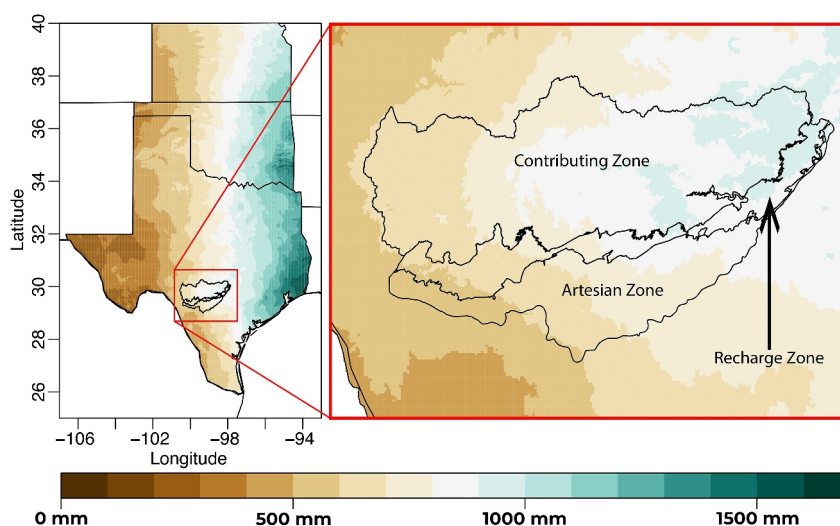


**Figure 1.** 1980–2014 climatology of average annual precipitation (P) across the Southern Great Plain region (left) and in the downscaling region (the Edwards Aquifer Region, right).

## 2.2. Observation and Global Climate Model Data

The observation data used in this study is the Daymet version 4 (Thornton et al., 2022, hereafter Daymet) which provides gridded observations of daily Tmax, daily Tmin, and daily total P at  $\sim 1$  km spatial resolution, starting 1 January 1980, across North America. The Daymet data were reprojected from their native map projection to a geographic projection using the functions available in the raster package (v 3.3–13) in R. Climate data is derived using 33 GCMs from the Coupled Model Intercomparison Project (CMIP) Phase 5 (CMIP5, Andrews et al., 2012) and 23 GCMs from Phase 6 (CMIP6, Eyring et al., 2016). The number of models used for downscaling was initially reduced to five each from CMIP5 and CMIP6 via the ensemble subset selection approach discussed in the next section. The list of models initially considered is provided in Table S1 of Supporting Information S1.

## 2.3. Ensemble Subset Selection Approach

The ensemble subset selection approach used in this study is based in part on the work of McSweeney et al. (2015) and Parding et al. (2020). The subset selection approach is described here with regards to its use to select a subset of models for statistical downscaling of daily high temperature (Tmax), daily low temperature (Tmin), and daily total precipitation (P) for the EAR.

### 2.3.1. Data Preparation

Several data preparation steps are implemented prior to starting the ensemble subset selection. First, for each GCM, the climatology of annual total P, annual average Tmax, and annual average Tmin are calculated for the respective historical periods of each ensemble (1980–2005 for CMIP5 and 1980–2014 for CMIP6). Second, the climatology of all three variables from all models is interpolated using bilinear interpolation to the Daymet grid and cropped to the SGP region. Third, the first two steps are repeated to create the climatology of all three variables for a future period (2070–2099) under the RCP 8.5 for the CMIP5 ensemble and the SSP 5–8.5 for the CMIP6 ensemble. The choice to use the end-century and high emission scenarios for subset selection is based on maximizing the change signal and potential spread of the ensemble. Fourth, the projected change of each variable from each GCM in the SGP region is calculated using historical and future climatology. The historical climatology and projected change are used with the ensemble subset selection approach to identify a subset of five GCMs from both the CMIP5 and CMIP6 ensembles that represent a range of future uncertainty while accurately representing the seasonality and magnitude of historical data for a region. Selection of a subset of models that meet specific performance criteria can reduce the computational burden needed to assess a multitude of models, especially given the often wide range of uncertainty across the full ensemble of model results, which can hinder effective decision making in assessing likelihood of future conditions. Recent literature suggests that some “hot-models” (those GCMs with a high equilibrium climate sensitivity [ECS]) should be removed from use

(Hausfather et al., 2022). However, a GCM with a high ECS values does not automatically make it an outlier for regional projected changes, particularly when incorporated into an impact assessment (Rahimpour Asenjan et al., 2023). As such, we retained all GCMs for this subset selection, regardless of their ECS value.

### 2.3.2. Historical Error Calculation

The first component of the ensemble subset selection approach is to determine the error of the historical climatology of all possible combinations of five model ensemble subsets. For this first component, the approach determines which ensemble subset minimizes the historical error. For each possible ensemble subset and a given variable, the historical climatology for the five GCMs are averaged together to produce a subset mean climatology. For each possible subset, the historical error is the normalized root mean square error (NRMSE) of the subset mean climatology compared to the Daymet observations:

$$NRMSE_s = \frac{\sqrt{\sum_{i=1}^N (M_i - O_i)^2}}{\sqrt{N}\sigma_O} \quad (1)$$

where  $M$  is the subset mean climatology, and  $O$  is the historical climatology from Daymet. The  $RMSE$  of ensemble subset  $s$  is determined as the square root of the mean squared errors from each of the  $i$ th grid cells, where  $N$  is the total number of grid cells. The  $NRMSE$  of subset  $s$  is calculated as the  $RMSE$  of subset  $s$  divided by the standard deviation ( $\sigma$ ) of the historical observations. The resulting  $NRMSE$  reflects the skill of the ensemble subset for a given variable across the SGP, which is in line with scale of information provided by GCMs.

### 2.3.3. Future Spread Calculation

The second component of the ensemble subset selection approach is to determine how much of the future spread in the ensemble is captured by the subset. This is accomplished using the fractional range coverage ( $FRC$ ) calculated similarly to that described by McSweeney et al. (2015) and Parding et al. (2020). At each grid cell in the SGP region, the  $FRC$  is calculated by

$$FRC_{s,i} = \frac{(max_{s,i} - min_{s,i})}{(max_{full,i} - min_{full,i})} \quad (2)$$

where  $s$  is the ensemble subset,  $i$  is the grid cell, and  $max$  and  $min$  are the maximum and minimum projected change, respectively. The numerator of Equation 2 is the range of projected change from a given subset  $s$  for grid cell  $i$ . The denominator of Equation 2 is the range projected change for grid cell  $i$  from the full ensemble. The  $FRC$  across all grid cells are averaged together to create a single  $FRC$  value for ensemble subset  $s$  via

$$FRC_s = \frac{\sum_{i=1}^N FRC_{s,i}}{N} \quad (3)$$

The  $NRMSE$  and  $FRC$  reflect the skill and spread, respectively, of each individual ensemble subset. Like the  $NRMSE$  calculation, the  $FRC$  is aggregated to one value for the SGP to reflect the ability of the subset to capture the spread of ensemble changes across the larger region, which is more in line with the scale of information provided by GCMs.

### 2.3.4. Multivariate Combination and Ensemble Subset Selection

The final component of the ensemble subset selection approach focuses on determining which ensemble subset minimizes the  $NRMSE$  and maximizes the  $FRC$ . Ideally, the minimum  $NRMSE$  is zero, representing a subset that perfectly captures the historical climatology, and the maximum  $FRC$  is one, representing a subset that has the same future spread as the full ensemble. Therefore, the subset selection approach calculates the Euclidean distance ( $D$ ) of each subset from the ideal situation using the  $NRMSE$  and  $FRC$  values from each subset using



$$D_s = \sqrt{(NRMSE_s - 0)^2 + (FRC_s - 1)^2} \quad (4)$$

In this study, we implemented the multivariate subset selection approach. The value of  $D$  is calculated for each subset  $s$  and variable  $v$ . Following a similar approach to Sanderson et al. (2017), the values of  $D$  for a given subset  $s$  over multiple variables can be combined using linear combination by

$$\Delta_s = \sum_{v=1}^V \frac{D_{s,v}}{V} \quad (5)$$

where  $\Delta_s$  is the multivariate distance for subset  $s$ ,  $v$  is the climate variable,  $V$  is the total number of climate variables, and  $D$  is the Euclidean distance for a given variable  $v$  and subset  $s$ . In the multivariate selection approach, the subset with the minimum multivariate distance is used. We applied the approach detailed in this section separately for the CMIP5 and CMIP6 ensembles, resulting in two separate five member ensembles that are then statistically downscaled for the EAR. This final step represents a departure from the approach of Parding et al. (2020), which used skill scores and user-defined weights to rank individual GCMs, where this study uses a multivariate distance (Equation 5) to select a GCM subset to capture skill and spread for the SGP region. This larger region is the focus of subset selection to minimize the error of GCM representation of larger scale patterns that affect the EAR while capturing the spread of changes from the GCM ensemble. A subset of five GCMs from each ensemble was chosen in consultation with the EAA to limit computational demands for the subsequent use of the projections in groundwater and spring flow modeling.

## 2.4. Downscaling Technique

### 2.4.1. Equidistant Quantile Mapping (EDQM) and Equi-Ratio Quantile Mapping (ERQM)

The downscaling techniques used for statistical downscaling of climatic features from GCMs for the EAR are equidistant quantile mapping (EDQM) and its variant known as equi-ratio quantile mapping (ERQM). We implemented these techniques for the EAR following the same procedures described by Wootten et al. (2020). The EDQM was used to produce downscaled projections of daily Tmax and Tmin. The ERQM was used to produce downscaled projections of daily total P. In addition, while the two techniques are subtly different, they share the same basic procedure. As such, we refer to the downscaling and results from the downscaling procedure as EDQM in the results and discussion sections.

#### 2.4.1.1. Equidistant Quantile Mapping (EDQM)

The EDQM approach, used for downscaling daily Tmax and Tmin, has been similarly applied in several other studies (Cannon et al., 2015; Lanzante et al., 2019; Li et al., 2010). For the downscaling in this study, we followed the procedure used in Dixon et al. (2020). The EDQM approach for downscaling daily Tmax and Tmin is mathematically equivalent to the quantile delta mapping (QDM, Cannon et al., 2015). The downscaling in this study makes use of the implementation of EDQM available in the MBC R Package (GitHub—cran/MBC), which reflects the EDQM method created by Li et al. (2010). The calculation is summarized below with specific notes for its application in this study.

The EDQM has four major steps. First, the cumulative distribution function (CDF) of the GCM-projected climatic feature values is determined for a given climatic variable, and then the corresponding quantile levels are computed by

$$\tau_{m,p} = F_{m,p}(x_{m,p}) \quad (6)$$

The second step is to calculate the change factor ( $\Delta$ ) between the simulated projected climatic feature values and the simulated historical climatic feature values from the GCMs at quantile levels by

$$\Delta_m = x_{m,p} - F_{m,h}^{-1}(\tau_{m,p}) \quad (7)$$

Third, the downscaled projected climatic feature values are determined by first estimating historical climatic feature values from the GCM-projected climatic feature values using the inverse CDF of the observed historical climatic feature values. Finally, the change factor, determined in Equation 7, is added to the estimated historical climatic feature values, as described below.

$$\hat{x}_{o,m,h;p} = F_{o,h}^{-1}(\tau_{m,p}) \quad (8)$$

$$\hat{x}_{o,p} = \hat{x}_{o,m,h;p} + \Delta_m \quad (9)$$

where  $m$  is the GCM-modeled value of the climate variable,  $p$  is the GCM-projected value of the climate variable,  $o$  is the observed historical value of the climate variable,  $h$  is the GCM-modeled historical value of the climate variable,  $\tau$  is the quantile level,  $F_{m,p}$  is the CDF of the GCM-modeled future variable,  $F_{o,h}$  is the CDF of the observed historical value of the variable,  $\Delta_m$  is the change factor, and  $\hat{x}_{o,p}$  is the downscaled value of the target variable.

In line with the previous work by Dixon et al. (2020), we applied the EDQM using a monthly time window with a 2-week overlap. For example, the values of  $\Delta_m$  for July were calculated using the month of July, the final 2 weeks of June, and the first 2 weeks of August. The use of a monthly time window enables a more accurate representation of seasonal variability in the downscaled climatic features in the region.

#### 2.4.1.2. Equi-Ratio Quantile Mapping (ERQM)

The ERQM is a variation of the EDQM that uses a multiplicative rather than an additive approach to determine and apply the change factors. The implementation used here is the same as in Dixon et al. (2020), Wootten et al. (2020), and Lanzante et al. (2021). The ERQM procedure is similar to the EDQM procedure except that Equations 7 and 9 are replaced by

$$\Delta_m = \frac{x_{m,p}}{F_{m,h}^{-1}(\tau_{m,p})} \quad (10)$$

$$\hat{x}_{o,p} = \hat{x}_{o,m,h;p} * \Delta_m \quad (11)$$

The ERQM variation of EDQM is applied for downscaling daily P because the multiplicative change factor prevents the downscaled P from having negative values. We also applied the ERQM with seasonal time window, following the work of Wootten et al. (2020), in order to provide enough non-zero P days to construct a robust CDF. Prior to the execution of ERQM, a trace adjustment similar to Pierce et al. (2015) was applied to correct the wet-day fraction of the modeled precipitation data to match that of the Daymet observations. In addition, prior to implementing ERQM a cube root transformation was applied to precipitation to yield a more Gaussian distribution. The ERQM was performed on the transformed P data, and the reverse transformation was applied to the results of ERQM.

#### 2.4.2. Training Period and Output Resolution

The training period for the statistical downscaling is different for the CMIP5 and CMIP6 ensemble subsets. The Daymet data, available from 1980 onward, limits the training period for both ensembles. The respective GCM ensembles have different historical simulation periods. The historical simulation period for the CMIP5 and CMIP6 ensembles end in 2005 and 2014, respectively. Thus, for the CMIP5 ensemble, the training period is 1980–2005, while the training period for the CMIP6 ensemble is 1980–2014. The output resolution of the projections matches the resolution of the Daymet data used in training (~1 km).

#### 2.4.3. Future Pathways and Period

Due to the slightly different training periods and the variations in emissions scenarios between CMIP5 and CMIP6, the future period between two ensembles differs. The future period of available downscaled projections using CMIP5 and CMIP6 GCMs is 2006–2099 and 2015–2099, respectively. In this study, we used CMIP5 GCM output created using representative concentration pathways (RCPs) 4.5 and 8.5 (Riahi et al., 2007; van Vuuren

**Table 1**  
*Mean Absolute Errors for the Full Ensemble and All Subsets for all Three Variables of Interest*

Variable	Group	Mean absolute error (full ensemble)	Mean absolute error (ensemble subset)
Tmax (°C)	CMIP5	−1.2	−0.72
	CMIP6	−0.7	−0.5
Tmin (°C)	CMIP5	2.0	1.1
	CMIP6	2.89	1.78
P (mm)	CMIP5	26.67	3.56
	CMIP6	12.95	7.11

et al., 2011) and CMIP6 GCM output created using shared socioeconomic pathways (SSPs) 2–4.5 and 5–8.5 (O’Neill et al., 2016). The RCP 4.5 and SSP 2–4.5 scenarios assume that the current energy production and use, and mitigation and adaptation strategies remain the same or similar in the future. Conversely, the RCP 8.5 and SSP 5–8.5 scenarios depict a worst-case situation, wherein future energy production heavily relies on fossil fuels, with minimal attention given to mitigation and adaptation measures. Consequently, the RCP 4.5 and SSP 2–4.5 represent intermediate emission scenarios, while RCP 8.5 and SSP 5–8.5 represent high emission scenarios.

### 3. Results

#### 3.1. Ensemble Subset Selection

The ensemble subset selection approach detailed in Section 2.3 was applied to the CMIP5 and CMIP6 ensembles to select five models from each ensemble for use in the statistical downscaling. The five GCMs chosen to form the ensemble subsets have a mean absolute error similar to, or less than, that of the full ensemble for all three variables to be downscaled for the EAR (Table 1). The spatial pattern and direction of the error of the ensemble subsets is similar to the full ensemble for total annual P (Figure S2 in Supporting Information S1), annual average of daily Tmax (Figure S3 in Supporting Information S1), and annual average of daily Tmin (Figure S4 in Supporting Information S1). The ensemble subset selection approach is designed to select GCMs that minimize historical error while maximizing the spread of projected changes for all three climate variables for the SGP region. The latter portion of the approach aims to capture as much of the uncertainty of climate projections associated with the GCMs as possible. The results from the ensemble subset selection for the SGP show that the ensemble subset captured most, if not all, the spread of the full ensemble for all three variables (Figure 2).

#### 3.2. Downscaling for the Edwards Aquifer Region

Next, we analyze the representativeness of the historical downscaled climate data (Tmax and P) for the EAR. In Figure 3, we compare the seasonal cycles of Tmax and P over the historical period from downscaled CMIP5 and CMIP6 models with the seasonal cycles from the Daymet historical data. While the downscaled Tmax from CanESM2 and CanESM5 are comparable to the observations from Daymet, the downscaled P from CanESM2 and CanESM5 do not reasonably represent the seasonality of P in the EAR.

Prior research indicates that ERQM and similar statistical downscaling techniques produce output that is time synchronous with the driving GCM (Wootten et al., 2020). This is different from a delta method for statistical downscaling where the output is time synchronous with the observations used for training. In other words, ERQM and similar methods incorporate dynamic changes in weather sequences from a GCM into the downscaled output. However, this also implies that incorrect seasonal cycles in a GCM can be translated into downscaled output. As a result of this effect, CanESM2 and CanESM5 were excluded from subsequent analyses.

To compensate for the exclusion of the two GCMs, we included two additional GCMs from CMIP6 models (INM-CM-8 and INM-CM-5.0) that exhibit similar magnitudes and seasonality for P as the other CMIP6 models. Consequently, we used four GCMs from the CMIP5 ensemble subset and six GCMs from the CMIP6 ensemble subset in the subsequent analyses and for use by the EAA. The historical and projected annual mean daily Tmax and daily total P from the CMIP5 and CMIP6 ensemble subsets under the intermediate and high emission scenarios along with the uncertainty bands for the San Antonio International airport (SAT) are shown in Figure S5 of Supporting Information S1, as an example.



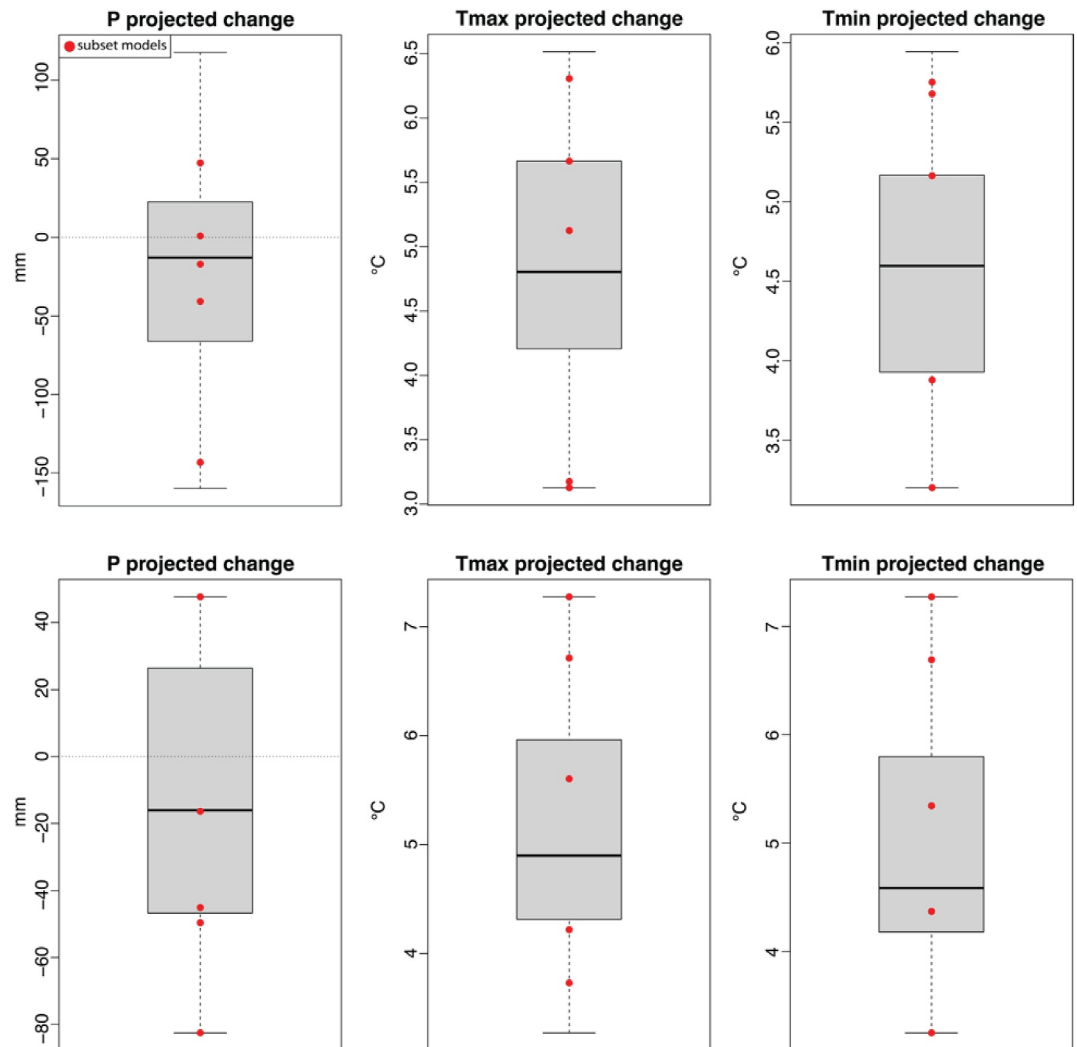


**Figure 2.** Spread of projected changes by the end of the century (2070–2099) for the CMIP5 (top row) and CMIP6 (bottom row) ensembles and subsets for the Southern Great Plains National Climate assessment (NCA) region. Boxplots represent the full ensemble of models available, while the red dots are the models selected for downscaling.

### 3.2.1. Historical Error

A fundamental purpose of statistical downscaling is to reduce the biases of the GCM output for a particular region, typically referred to as bias-correction. For both P and Tmax, the spatial RMSE of the ensemble subsets downscaled by EDQM is much less than the spatial RMSE of the raw ensemble subset (RMSE is 76%–99% smaller for the CMIP5 ensemble and 54%–99% smaller for the CMIP6 ensemble). The mean error and root mean square error (RMSE) of P in each individual model were also reduced by the implementation of EDQM (Table 2). The error of Tmax and Tmin was also reduced by the EDQM both for the mean subset and for the individual models in each subset (Tables 3 and 4). There is also improvement in the spatial distribution of error of the raw GCM ensemble subsets. The raw CMIP5 and CMIP6 ensemble subsets exhibit a tendency to overestimate P in the western and southern portions of the domain, underestimate P in the central and northeastern portions, and underestimate Tmax (Figure S6 in Supporting Information S1). The raw ensemble subsets also tended to overestimate Tmin (Figure S7 in Supporting Information S1) in the EAR.

### 3.2.2. Projected Changes

The downscaled ensemble subsets provide EAR-specific guidance on potential climatic changes. The available projections cover the period of 2006–2099 for CMIP5 and 2015–2099 for CMIP6. In this section, we focus on

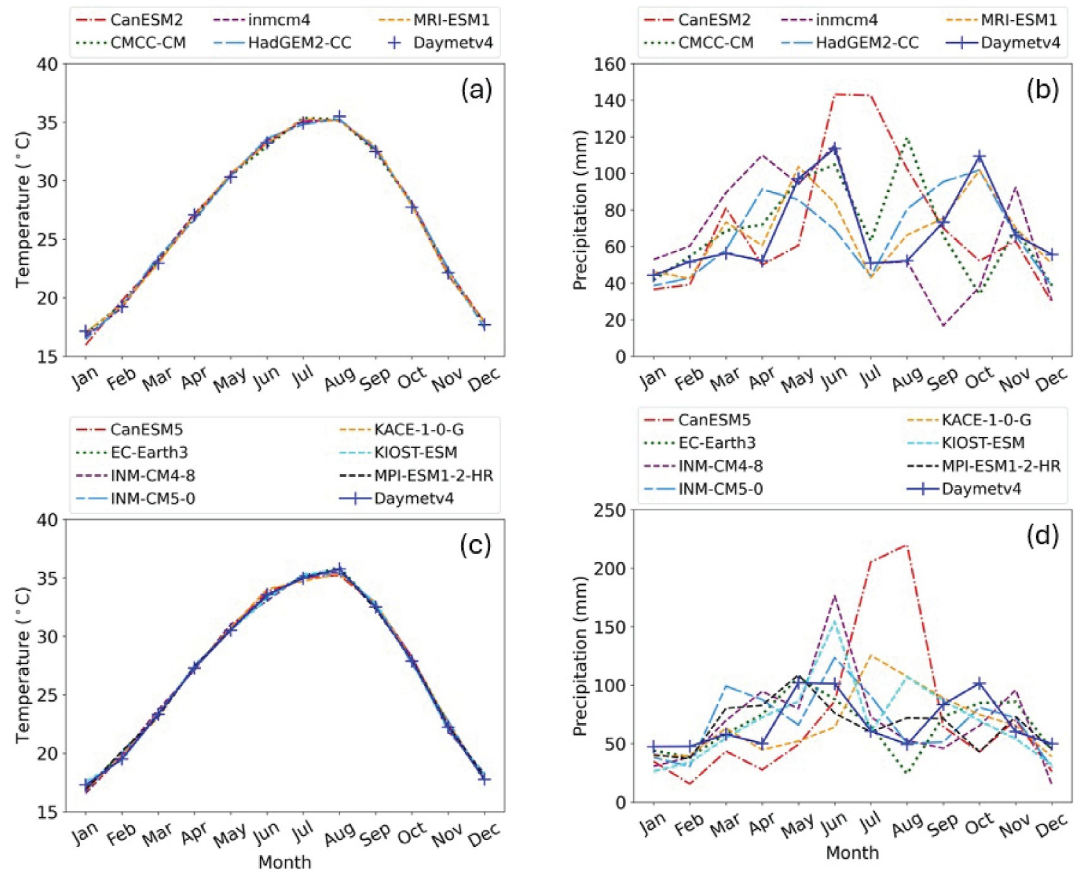


**Figure 3.** Comparison of monthly variations in historical Tmax and P from the downscaled CMIP5 ensemble subset (a–b) and the downscaled CMIP6 ensemble subset (c–d) to Daymet data at the San Antonio International Airport (SAT) location.

the projected changes during the mid-century (2036–2065) and end-century (2070–2099). These two periods are commonly used for calculating projected changes in the National Climate Assessment (NCA). Because the MRI-ESM1 was not run using the RCP 4.5 as an input, projected changes from the CMIP5 subset with RCP 4.5 consists of three models, while the CMIP5 subset with RCP 8.5 includes four models.

**Table 2**

Mean Error and Root Mean Square Error for All Subset Models for the EAR Annual Precipitation (P, mm) Pre-Downscaling (Pre-DS) and Post-Downscaling (Post-DS)

Group	Model	Mean error		Root mean square error	
		Pre-DS	Post-DS	Pre-DS	Post-DS
CMIP5	CMCC-CM	−48.78	−2.83	91.34	14.07
	HadGEM2-CC	41.47	0.53	124.58	10.42
	inmcm4	−61.94	−27.78	129.01	29.88
	MRI-ESM1	94.46	−3.91	139.55	6.33
CMIP6	EC-Earth3	200.16	−4.04	204.4	7.8
	INM-CM-4-8	−16.51	31.25	110.72	33.73
	INM-CM-5-0	5.96	17.25	100.24	46.39
	KACE1-0-G	27.46	8.82	82.8	13.82
	KIOST-ESM	121.09	27.9	162.37	30.34
	MPI-ESM1-2-HR	−194.5	−1.52	215.87	8.36

### 3.2.2.1. Projected Temperature Changes

The ensemble-mean projected changes in Tmax are notably larger in the CMIP6 subset than in the CMIP5 subset (Figure 4). Despite a slight temperature change gradient from west to east in the EAR, the projected increases are similar across the region. For mid-century under intermediate emissions (RCP 4.5 and SSP 2–4.5), the mean projected changes in Tmax range from 1.68°C to 2.18°C. By end-century under the same emissions, the projected changes in Tmax increase to 2.2°C and 2.64°C. For mid-century under high emissions (RCP 8.5 and SSP 5–8.5), the mean projected changes in Tmax range from 2.08°C to 2.66°C. For end-century under high-emission scenarios, the mean projected changes in Tmax further increase to 4.25°C–4.3°C.

Projected increases in temperature extremes follow similar patterns to the projected increases in Tmax. The average annual number of days with high temperatures over 100°F (37.78°C, Tmax100) is projected to increase in the EAR, with the greatest increases in the southern portion of the region and the smallest increases in the higher elevation regions in the western and northern

**Table 3**  
Mean Error and Root Mean Square Error for All Subset Models for the EAR Annual Average High Temperature ( $T_{max}$ , °C) Pre and Post Downscaling

Group	Model	Mean error		Root mean square error	
		Pre-DS	Post-DS	Pre-DS	Post-DS
CMIP5	CMCC-CM	-0.76	-0.02	0.86	0.02
	HadGEM2-CC	-2.74	-0.002	2.93	0.003
	inmcm4	-0.3	-0.01	1.1	0.01
	MRI-ESM1	-3	0.009	3	0.009
CMIP6	EC-Earth3	-2.47	0.02	2.5	0.02
	IN-MCM-4-8	0.61	0	1.21	0.01
	IN-MCM-5-0	0.32	-0.01	1.03	0.01
	KACE1-0-G	0.02	-0.02	0.85	0.02
	KIOST-ESM	-2.41	0.01	2.58	0.01
	MPI-ESM1-2-HR	0.03	0	0.58	0.01

portions of the region (Figure S8 in Supporting Information S1). For reference,  $T_{max100}$  is calculated for each grid cell and averaged to the EAR mean. The mean projected changes in  $T_{max100}$  during mid-century under intermediate emission scenarios are in the range of 18.76–43.15 days. The mean projected changes in  $T_{max100}$  by end-century under the same emission scenarios range from 26.63 to 42.45 days. The mean projected increase in  $T_{max100}$  during mid-century under high emission scenarios ranges from 30.27 to 51.07 days and 68.21–71.69 days by end-century. These results indicate a higher risk of experiencing more frequent and prolonged dry spells, potentially triggering the onset of droughts within the EAR under future climates, especially under high emission scenarios. The individual GCMs all suggest an increase in both  $T_{max}$  and  $T_{max100}$  across the region but with varying magnitudes (Table 5, Figures S9–S12 in Supporting Information S1). The results for  $T_{min}$  are similar to  $T_{max}$  in both magnitude and spatial patterns across the EAR (Figures S13–S15 in Supporting Information S1).

### 3.2.2.2. Projected Precipitation Changes

The mean projected changes in P within the EAR are more variable under different emission scenarios. In general, the CMIP5 subset projects higher P, while the CMIP6 subset projects less P. Under the intermediate emission scenarios, the CMIP5 subset projects the most substantial increase in P in end-century, while the CMIP6 subset projects the most significant decrease in P in mid-century. In particular, the CMIP6 subset projects less P, especially on the eastern side of the region, under both intermediate and high emission scenarios (Figure 5). The mean projected increases in P during mid-century under low emissions exhibit a broader variation, ranging from an increase of 27.23 mm (CMIP5) to a decrease of 40.85 mm (CMIP6). Under the same emission scenario, the mean P is projected to increase in the range of 1.28 mm (CMIP6) to 49.87 mm (CMIP5) during end-century. Under the high emission scenarios during mid-century, the mean projected range from a decrease of 14.55 mm (CMIP6) to an increase of 16.78 mm (CMIP5). However, under high emission scenarios during end-century, the mean P is projected to decrease in the range of 0.99 mm (CMIP6) and 19.88 mm (CMIP5).

The ensemble subsets indicate a negligible to small increase in 1-day maximum precipitation ( $rx1day$ ) with no clear spatial pattern (Figure S16 in Supporting Information S1). Under intermediate emissions in mid-century, the mean projected changes in  $rx1day$  are in the range of 8.26 mm (CMIP6) and 12.01 mm (CMIP5). In the end of the century under the same emissions scenario, the mean changes in  $rx1day$  range from 8.88 mm (CMIP6) to 9.81 mm

(CMIP5). Under high emissions during mid-century, the mean changes in  $rx1day$  are projected to be in the range of 6.06 mm (CMIP5) and 12.06 mm (CMIP6). Under the same emission scenarios, the mean projected changes in  $rx1day$  by the end of the century range from 10.30 mm (CMIP6) to 17.42 mm (CMIP5). Thus, unlike P, the mean projected changes in  $rx1day$  show little variation regardless of the emissions scenarios. The projected changes in P have a wide range reflecting the potential for both a drier or wetter future across the EAR, while the  $rx1day$  is projected to increase (Table 6, Figures S17–S20 in Supporting Information S1). The anomalies in regional average projected climatic features acquired from the CMIP5 and CMIP6 subsets under intermediate and high emission scenarios are summarized in Table 7.

**Table 4**  
Mean Error and Root Mean Square Error for All Subset Models for the EAR Annual Average Low Temperature ( $T_{min}$ , °C) Pre-Downscaling (Pre-DS) and Post-Downscaling (Post-DS)

Group	Model	Mean error		Root mean square error	
		Pre-DS	Post-DS	Pre-DS	Post-DS
CMIP5	CMCC-CM	1.94	-0.03	2.01	0.03
	HadGEM2-CC	-0.2	-0.02	1.04	0.02
	inmcm4	-4.01	-0.04	4.15	0.04
	MRI-ESM1	1.27	-0.007	1.46	0.008
CMIP6	EC-Earth3	1.07	-0.01	1.18	0.01
	IN-MCM-4-8	1.34	-0.01	1.7	0.02
	IN-MCM-5-0	1.26	-0.02	1.61	0.02
	KACE1-0-G	0.22	-0.06	1.22	0.06
	KIOST-ESM	0.1	-0.03	0.99	0.03
	MPI-ESM1-2-HR	3.74	-0.03	3.82	0.03

## 4. Discussion

The approach to creating customized downscaled projections for the EAR includes selecting a subset of GCMs, downscaling those chosen GCMs, determining historical error, and determining projected changes. In this case, the ensemble subset selection approach initially identified five GCMs from CMIP5 and five GCMs from CMIP6, collectively yielding comparable results to their respective full ensembles. These subsets were changed in consultation with EAA to remove those with unreasonable seasonal cycles of P. The

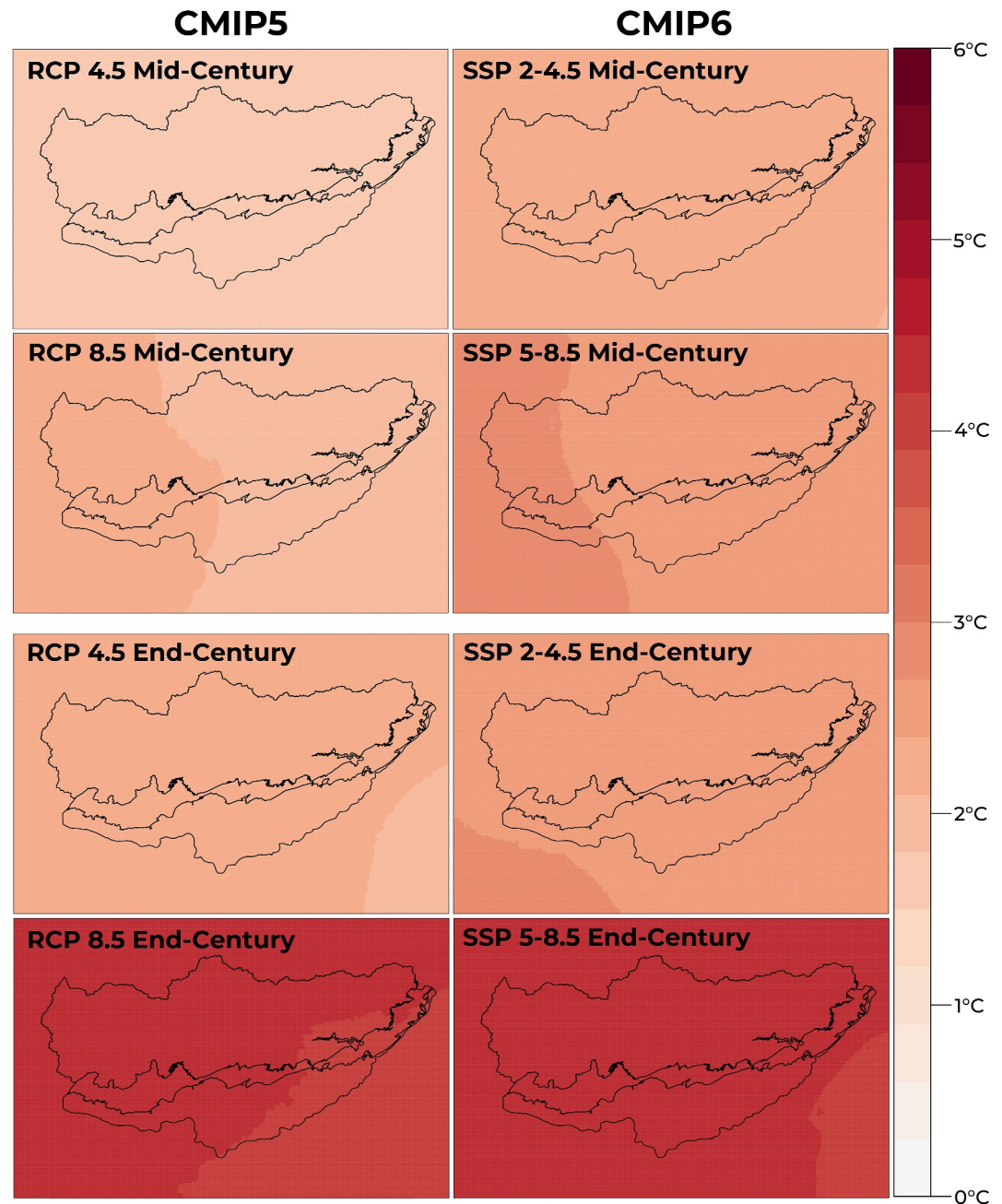


**Figure 4.** Mean projected changes in annual average high temperature ( $T_{max}$ ) for the mid-century (2036–2065) and end-century (2070–2099) from the downscaled CMIP5 (left) and CMIP6 (right) ensembles. CMIP5 ensemble includes the RCP 4.5 and RCP 8.5 scenarios. CMIP6 ensemble includes the SSP 2–4.5 and SSP 5–8.5 scenarios.

statistical downscaling reduced the error for the selected GCMs for all three variables. According to the ensembles of downscaled projections (Table 7), the average daily  $T_{max}$  is projected to increase by  $1.93^{\circ}\text{C}$ – $2.37^{\circ}\text{C}$  on average by mid-century and  $2.42^{\circ}\text{C}$ – $4.27^{\circ}\text{C}$  on average by end-century. These changes are similar for  $T_{min}$ . The projected changes in  $P$  exhibited greater variations between the CMIP5 and CMIP6 ensembles. According to the CMIP5 downscaled ensembles, average total  $P$  in the EAR is projected to increase by 16.78–27.23 mm on average by mid-century. The CMIP5 ensembles also project  $P$  to increase by 49.87 mm on average (intermediate scenarios) and decrease by 19.88 mm on average (high scenarios) by end-century. According to the CMIP6 downscaled ensembles,  $P$  is projected to decrease by 14.55–40.85 mm on average by mid-century. The CMIP6 ensembles project little change in  $P$  (decrease by 0.99 mm to increase of 1.28 mm) by end-century. Thus, during



**Table 5**  
*Projected Changes in Annual Average High Temperature (Tmax, °C) and Annual Average Number of Days Tmax ≥100°F (Tmax100, Days) for All Models Across the EAR*

Group	Model	Intermediate emission scenario (RCP 4.5 and SSP 2–4.5)				High emission scenario (RCP 8.5 and SSP 5–8.5)			
		Tmax		Tmax100		Tmax		Tmax100	
		Mid-century	End-century	Mid-century	End-century	Mid-century	End-century	Mid-century	End-century
CMIP5	CMCC-CM	1.85	2.8	24.84	38.68	2.33	5.58	37.9	104.76
	HadGEM2-CC	2.67	3.23	28.85	37.32	3.23	5.3	41.67	86.11
	inmcm4	0.51	0.57	2.58	3.9	1.11	2.8	13.62	29.9
	MRI-ESM1	NA	NA	NA	NA	1.66	3.3	27.89	52.07
CMIP6	EC-Earth3	2.77	3.72	57.23	64.79	3.64	5.9	78.92	106.3
	INM-CM4-8	1.85	1.9	31.9	28.86	2.41	3.95	38.15	55.83
	INM-CM5-0	1.7	1.92	25.9	35.13	2.16	3.24	32.47	45.46
	KACE1-0-G	2.72	3.3	43.11	35.06	3.15	4.9	51.87	76.53
	KIOST-ESM	2.55	2.78	73.34	63.84	2.74	4.03	74.2	87.61
	MPI-ESM1-2-HR	1.49	2.19	27.44	27.02	1.88	3.79	30.8	58.38

the projected warmer temperatures in the EAR, while CMIP5 ensemble projects increased precipitation, CMIP6 ensemble project reduced precipitation by mid-century under both intermediate and high emission scenarios. However, under persistently warming temperatures by end-century, while CMIP5 and CMIP6 ensembles project increased precipitation under the intermediate emission scenario, they project reduced precipitation under the high emission scenario. Increasing temperatures will likely lead to a net increase in evapotranspiration though this was not formally evaluated in this study.

Our findings align with earlier studies that used previous generations of GCMs and noted projected increases in Tmax and decreases in P (e.g., Loáiciga, 2009; Loáiciga et al., 2000), and projections from two National Climate Assessments (Kloesel et al., 2018; Marvel et al., 2023). *A key finding is that the temperatures will likely increase in the EAR with a corresponding increase in the frequency of very hot days, which will increase evapotranspiration. These factors are poised to intensify the frequency and severity of drought conditions in the EAR under the changing climate.* More frequent drought conditions could lead to decreased groundwater availability, reduced spring flow, and elevated surface water temperatures. Such shifts pose challenges for aquifer management, especially with population growth and required sustainable environmental flow for karstic spring ecosystems. Our findings are consistent with those of Loáiciga et al. (2000); Loáiciga (2009), which suggest that the Edwards Aquifer's groundwater resources could be at risk in a changing climate, particularly without rigorous mitigation efforts. This study builds upon and refines the approach taken by Loáiciga et al. (2000); Loáiciga (2009) in integrating climate projections for the EAR. Their research employed a change factor (or delta method), applying uniform change factors to historical temperature and precipitation data, remains time-synchronous with the historical observations. However, it does not capture the dynamic variability in weather patterns provided by GCMs, thereby artificially limiting variability in rain events and maintaining the original distribution shape. In contrast, the EDQM downscaling in our approach to addressing the needs of the EAA allows for a nuanced representation of changes, including alterations in the tails of the distribution indicated by the GCM (Wootten et al., 2020), which is crucial for accurate hydrological modeling of the Edwards Aquifer. The downscaled climate projections also indicate an increase in 1-day maximum P but fewer rainy days on average. These changes may weaken diffuse recharge while enhancing the role and impact of focused recharge. Moreover, as precipitation events become more intense and less frequent, the likelihood of flooding increases due to larger amounts of runoff and reduced soil absorption. In addition, the projections produced in this study provided added confidence to existing projections for the region and the necessary resolution for future assessments of projected changes in groundwater levels and springs flow in the EAR. The climate projections generated in this work will be integral to future groundwater and spring flow modeling efforts in the Edwards Aquifer and will be presented as part of our follow-up research.

A noteworthy aspect of this study is the comparison between the CMIP6 and CMIP5 model ensembles with a larger projected temperature increase in the CMIP6 ensemble. This difference suggests a discussion of the “hot



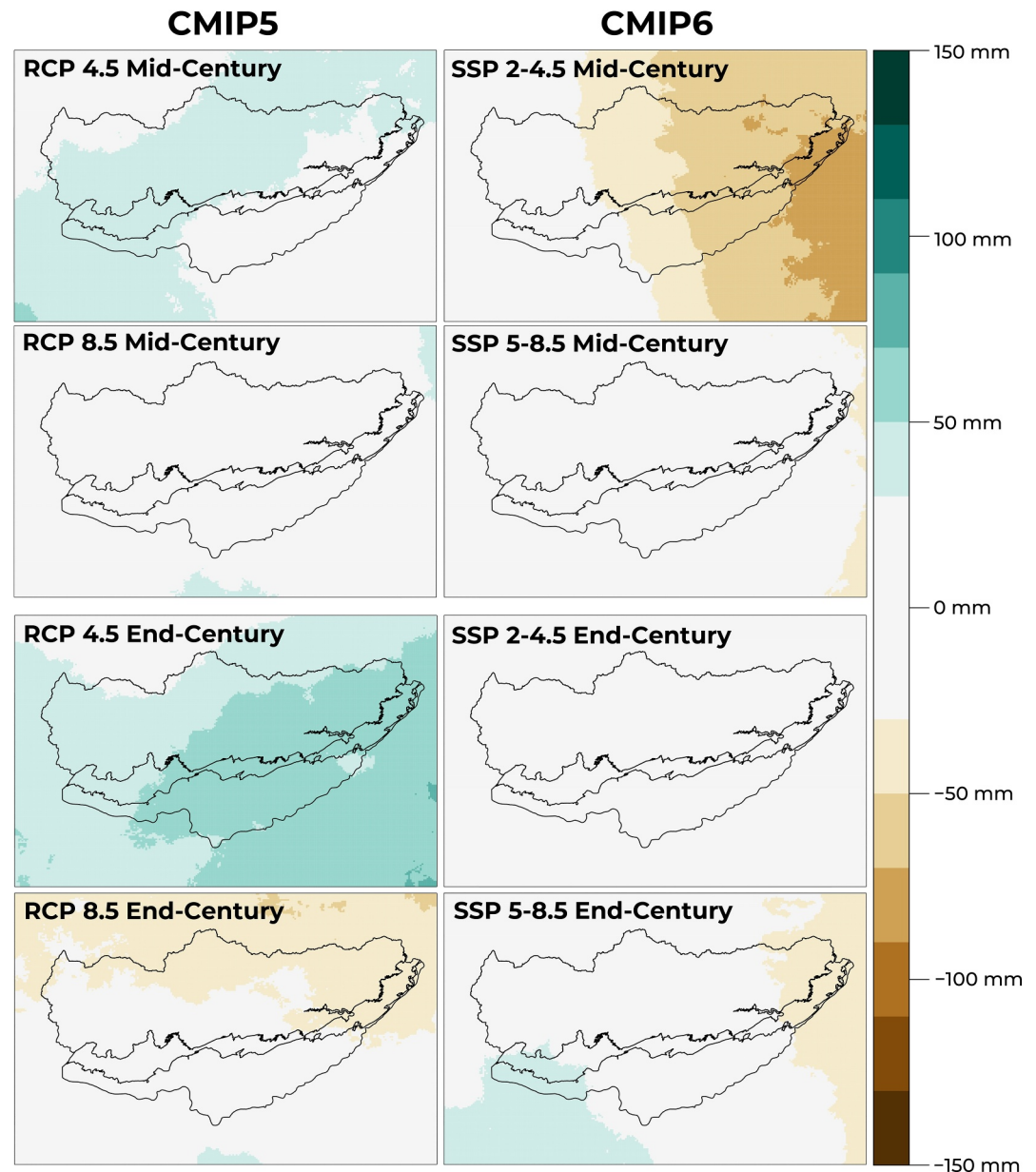


**Figure 5.** Mean projected changes in average annual total precipitation (P) for the mid-century (2036–2065) and end-century (2070–2099) from the downscaled CMIP5 (left) and CMIP6 (right) ensembles. CMIP5 ensemble includes the RCP 4.5 and RCP 8.5 scenarios. CMIP6 ensemble includes the SSP 2–4.5 and SSP 5–8.5 scenarios.

model” issue is warranted. Some CMIP6 models, termed “hot models,” exhibit an ECS that exceeds the range deemed “very likely” (between 2°C and 5°C) by the Intergovernmental Panel on Climate Change’s Sixth Assessment Report (AR6, Hausfather et al., 2022). Hausfather et al. (2022) recommend excluding models that fall outside this “very likely” ECS range, as they may overestimate the sensitivity to emissions scenario-induced forcing changes. This aspect highlights the importance of model selection and interpretation in climate studies with regards to the “practitioner’s dilemma”.

The ensemble subset selection approach focused on how effectively each potential subset captured the historical climatology of three variables across the Southern Great Plains (SGP) and the range of projections in the full ensemble. Except for CanESM5, selected GCMs fall within the “very likely” ECS range suggested by AR6 report (Table S2 in Supporting Information S1). ECS is a global metric that quantifies the global average temperature increase expected after the climate system stabilizes following a doubling of atmospheric carbon dioxide levels.

**Table 6**  
Projected Changes in Annual Precipitation (P) and 1-Day Maximum Precipitation (rx1day) (mm) for all Models Across the EAR

Group	Model	Intermediate emission scenario (RCP 4.5 and SSP 2–4.5)				High emission scenario (RCP 8.5 and SSP 5–8.5)			
		P		rx1day		P		rx1day	
		Mid-century	End-century	Mid-century	End-century	Mid-century	End-century	Mid-century	End-century
CMIP5	CMCC-CM	39.73	44.73	18.14	12.36	−28.36	−167.52	12.01	13.97
	HadGEM2-CC	27.25	19.54	12.72	11.49	29.87	12.4	6.5	18.14
	inmcm4	14.71	85.34	5.16	5.57	27.1	1.45	4.9	17.74
	MRI-ESM1	NA	NA	NA	NA	38.52	74.15	0.81	19.82
CMIP6	EC-Earth3	−12.88	−53.78	15.13	9.48	−32.97	−54.06	12.28	19.06
	INM-CM4-8	−93.45	94.85	0.084	8.81	−57.89	10.61	1.17	2.6
	INM-CM5-0	−62.22	21.86	0.98	4.09	27.09	209.62	8.29	25.99
	KACE1-0-G	34.95	84.02	13.86	16.48	96.42	38.21	28.78	7.85
	KIOST-ESM	−69.94	−53.35	10.75	12.55	−68.53	−79.74	5.1	−2.53
	MPI-ESM1-2-HR	−41.53	−85.93	8.73	1.84	−51.4	−130.57	16.73	8.8

The ability of a GCM to accurately represent this global sensitivity metric does not necessarily correlate with ability to capture regional physical processes or impacts of large-scale climatic changes, particularly for precipitation projections. For example, the EC-Earth3 and KACE1-0-G have a similar ECS value, but the downscaled EC-Earth3 projects a precipitation decrease in the EAR while the downscaled KACE1-0-G projects an increase in the EAR (Table S2 in Supporting Information S1). *This finding highlights a critical aspect: the ECS values of the subset models may not necessarily have a strong relationship with regional precipitation projections post-downscaling. This underscores the importance of considering regional-specific dynamics and responses when selecting or creating decision-relevant climate projections.* Aligned with this critical observation, CanESM2 and CanESM5 were omitted from further analyses at the EAR-scale in this study, but their exclusion was not due to their ECS values, but because of their poor representation of the seasonality of historical regional precipitation within the EAR (see Figure S5 in Supporting Information S1), and this was deemed unacceptable with respect to the EAA's needs for climate projections.

Hydrological models are known for their complex and non-linear responses to temperature and precipitation changes (Chen et al., 2016; Ross & Najjar, 2019). Recent studies, including Rahimpour Asenjan et al. (2023), have explored the effects of excluding “hot models” from streamflow projections with mixed results. Omitting

“hot models” sometimes reduced the uncertainty in streamflow projections, in other instances, it either had no impact or even increased the uncertainty. This variability in outcomes underscores a second point for the challenge of the “practitioner's dilemma”: *GCMs outside the “very likely” ECS range may still, following downscaling and hydrology modeling, produce plausible projections of climate impacts for a specific application or decision-context.* This is likely because a GCM that is an outlier in terms of ECS may well not be an outlier for regional scale changes as is shown in our results (Table S2 in Supporting Information S1). Future research should delve into understanding the potential impacts of “hot models” on various climate-related aspects, such as aquifer recharge, particularly as the sample size in this study was small compared to other studies such as Rahimpour Asenjan et al. (2023). The current selection of projections discussed in this study represents a diverse range of projections that will be integral to our ongoing efforts in groundwater and spring flow modeling within the Edwards Aquifer. This approach ensures a comprehensive and nuanced understanding of climate impacts on the EAR, considering a wide range of model sensitivities and scenarios.

Downscaled climate projections are subject to various sources of uncertainty, including uncertainties related to the GCMs, emissions scenarios, and the

**Table 7**  
Regional Average of Projected Changes in Climate Variables From CMIP5 and CMIP6 Subset Ensembles During Mid-Century and End-Century Under Intermediate Emission (RCP 4.5 and SSP 2–4.5) and High Emission (RCP 8.5 and SSP 5–8.5 Scenarios)

Time period	Variable	CMIP5		CMIP6	
		RCP 4.5	RCP 8.5	SSP 2–4.5	SSP 5–8.5
Mid-Century	Tmax	1.68	2.08	2.18	2.66
	P	27.23	16.78	−40.85	−14.55
	# of rain days	−1.70	−2.12	−3.80	−3.19
	rx1day	12.01	6.06	8.26	12.06
	Tmax100	18.76	30.27	43.15	51.07
End-Century	Tmax	2.20	4.25	2.64	4.30
	P	49.87	−19.88	1.28	−0.99
	# of rain days	−1.01	−7.73	−2.45	−4.33
	rx1day	9.81	17.42	8.88	10.30
	Tmax100	26.63	68.21	42.45	71.69

downscaling process itself (Hawkins & Sutton, 2009, 2011; Wootten et al., 2017). Additionally, the training data used in statistical downscaling introduces another layer of uncertainty (Pourmokhtarian & Driscoll, 2016; Wootten et al., 2020). It is generally observed that the uncertainty in downscaling is less significant than that in GCMs and scenarios, particularly concerning temperature projections. In addition, other studies have noted that the uncertainties of the hydrology models or other impacts models are themselves significant sources of uncertainty in climate impacts assessments (e.g., Chen et al., 2011; Giuntoli et al., 2018; Krysanova et al., 2018; Piotrowski et al., 2021; Trudel et al., 2017). While our downscaled projections do not incorporate a variety of downscaling techniques or multiple sets of gridded observations for training, the ensemble subset selection approach we employed effectively captures the GCM uncertainty within our CMIP5 and CMIP6 subset ensemble. Moreover, by utilizing multiple emissions scenarios, our projections also address scenario uncertainty. Thus, the projections generated in this study adequately encompass the key sources of uncertainty pertinent to future analyses. However, future research could benefit from considering multiple downscaling techniques or incorporating additional training data, particularly for the EAR or additional comparisons to pre-existing downscaled projections. This consideration is especially relevant for precipitation projections, where the uncertainty associated with the downscaling technique and training data tends to be more pronounced (e.g., Wootten et al., 2020). Such an expansion in methodologies and data sources would enhance the robustness and reliability of future climate impact assessments.

Overall, this study presents a complete approach to selecting and/or creating new projections in the decision-relevant context of the EAA. This approach allows for selecting a subset of GCMs to either downscale or work with from a pre-downscaled data set. In addition, this approach is flexible enough to allow for analytic selection and evaluation and for incorporating other insights or needs identified by an end-user for a given application. The approach described in this study is offered as an approach to addressing the “practitioner’s dilemma” that could be easily applied to other contexts and regions and offers the opportunity to address when new projections are needed alongside of selections from pre-existing projections. However, this approach is one of many, and it is beyond the scope of this project to compare approaches to determine best practices and standardized evaluation and selection protocols to address the larger challenge of the “practitioner’s dilemma.” This comparison remains a gap in the literature that is a critical need for the future use and development of decision-relevant climate projections. In addition, this method and other subset selection methods may also be sensitive to the resolution of the data used. This aspect in particular is the subject of future research by the authors.

Management of the Edwards Aquifer relies on several mitigation and conservation strategies designed to maintain adequate spring flow to ensure the viability of threatened and endangered species at two major spring systems. Specific spring flow rates (e.g., long-term average flows and minimum short-term flows) were established as part of the Edwards Aquifer Habitat Conservation Plan (RECON Environmental Inc. et al., 2012) and its associated Incidental Take Permit (ITP) (U.S. Fish and Wildlife Service, 2015). For example, the target 10-day average minimum spring flows at Comal and San Marcos springs are 0.85 m<sup>3</sup>/s (30 ft<sup>3</sup>/s) and 1.27 m<sup>3</sup>/s (45 ft<sup>3</sup>/s), respectively. The magnitude and sequence for implementing spring flow protection measures are based on sustaining minimum spring flows through conditions equivalent to the regional drought of record, which occurred in the 1950s. The current ITP expires in 2028, and its renewal will require explicit consideration of the potential effects of future climate on the groundwater system and spring flows. Thus, a particular concern is whether current mitigation measures will be adequate to ensure adequate spring flows under future droughts.

While the climate projections described here provide insight into future changes in the magnitude and frequency of stressors on the aquifer (e.g., increased temperatures and fewer days with precipitation), the projections must be used to produce estimates of aquifer recharge, which are then input to a groundwater flow model that incorporates pumping demand and implementation of mitigation strategies. Accurate estimation of recharge, particularly in the spatially complex karstic aquifer system, is enhanced through our downscaling process with finer discretization. The groundwater flow model will simulate water levels and spring flows over the proposed ITP renewal period for all 19 sets of projections. These results will be crucial for evaluating the adequacy of the current regulatory framework or identifying needs for changes in aquifer management. Recharge and groundwater flow modeling is currently in progress and results will be reported upon completion of these studies.

## 5. Conclusions

This study details an approach to addressing the “practitioner's dilemma” in the decision-context of the Edwards Aquifer Authority, resulting in the production of downscaled climate projections of daily high temperature, daily low temperature, and daily total precipitation for the Edwards Aquifer Region. The unique needs of the Edwards Aquifer Region required producing new downscaled projections rather than relying on pre-existing data sets. This is different from traditional studies in regards to the “practitioner's dilemma.” The process encompasses the selection of appropriate GCMs for downscaling and the downscaling process itself that can be flexibly applied to other regions and account for other insights. We utilized subset ensembles from the CMIP5 and CMIP6 GCMs with statistical downscaling correcting the errors in the chosen GCMs. Our newly developed data set projects significant climatic changes for the Edwards Aquifer Region. By the end of the century, the ensemble means of regional average temperatures are projected to rise by 2.0°C–4.3°C while annual precipitation is projected to vary from a decrease of 10.4 mm to an increase of 25.6 mm. A decrease in rainy days by up to 6 and an increase in the number of days with temperatures exceeding 37.8°C (100°F) of 35–70 days annually on average are also projected. Projected climatic stress in the region could have been worse if the downscaled climatic data from “hot models” were included in the regional climate analyses. They were omitted as they did not accurately represent the magnitude and seasonality of historical precipitation in the region. The projected climatic shifts are likely to increase heatwaves, dry spells, and evapotranspiration rates, thereby exacerbating the potential for development of drought conditions. This could lead to a reduction in the availability of groundwater within the Edwards Aquifer. The set of downscaled projections generated in this study will be pivotal in future groundwater and spring flow modeling. They will provide a robust and comprehensive understanding of the potential impacts of climate change on the Edwards Aquifer, aiding in the development of effective strategies to manage and mitigate these impacts. Moreover, this study presents an approach to addressing the “practitioner's dilemma,” advancing the discussion on the production of decision-relevant climate projections.

## Data Availability Statement

GCM data from CMIP5 and CMIP6 were accessed from the Earth System Grid Federation (ESGF) repositories, which are publicly accessible with registration (ESGF User Support Working Team, 2019). The Daymet version 4 data is publicly available from NASA EarthData and Oak Ridge National Laboratory (Thornton et al., 2022). R code for subsequent analyses is available via Zenodo (Wootten, 2024a). R Code for Ensemble Subset Selection Algorithm v 1.0 is also available via Zenodo (Wootten, 2024b). The downscaling makes use of the same code in the MBC R package (GitHub—cran/MBC, Cannon et al., 2015). The EAA is committed to providing the downscaled projections to interested users. However, the EAA has chosen not to provide a direct link or access to their data repository owing to security concerns. The EAA has granted permission to the South Central CASO to provide the EAR downscaled climate projections via the USGS ScienceBase (Wootten et al., 2024).

## References

- Abatzoglou, J. T., & Brown, T. J. (2012). A comparison of statistical downscaling methods suited for wildfire applications. *International Journal of Climatology*, 32(5), 772–780. <https://doi.org/10.1002/joc.2312>
- Andrews, T., Gregory, J. M., Webb, M. J., & Taylor, K. E. (2012). Forcing, feedbacks and climate sensitivity in CMIP5 coupled atmosphere-ocean climate models. *Geophysical Research Letters*, 39(9), 1–7. <https://doi.org/10.1029/2012GL051607>
- Barsugli, J., Guentchev, G., Horton, R. M., Wood, A., Mearns, L. O., Liang, X.-Z., et al. (2013). The practitioner's dilemma: How to assess the credibility of downscaled climate projections. *Eos Transactions*, 94(46), 424–425. <https://doi.org/10.1002/2013EO460005>
- Bhatt, G., Linker, L., Shenk, G., Bertani, I., Tian, R., Rigelman, J., et al. (2023). Water quality impacts of climate change, land use, and population growth in the Chesapeake Bay watershed. *JAWRA Journal of the American Water Resources Association*, 59(6), 1313–1341. <https://doi.org/10.1111/1752-1688.13144>
- Cannon, A. J., Sobie, S. R., & Murdock, T. Q. (2015). Bias correction of GCM precipitation by quantile mapping: How well do methods preserve changes in quantiles and extremes? *Journal of Climate*, 28(17), 6938–6959. <https://doi.org/10.1175/JCLI-D-14-00754.1>
- Chakraborty, D., Başağaoğlu, H., Gutierrez, L., & Mirchi, A. (2021). Explainable AI reveals new hydroclimatic insights for ecosystem-centric groundwater management. *Environmental Research Letters*, 16(11), 114024. <https://doi.org/10.1088/1748-9326/ac2fde>
- Chen, J., Brissette, F. P., & Leconte, R. (2011). Uncertainty of downscaling method in quantifying the impact of climate change on hydrology. *Journal of Hydrology*, 401(3–4), 190–202. <https://doi.org/10.1016/j.jhydrol.2011.02.020>
- Chen, J., Brissette, F. P., & Lucas-Picher, P. (2016). Transferability of optimally-selected climate models in the quantification of climate change impacts on hydrology. *Climate Dynamics*, 47(9–10), 3359–3372. <https://doi.org/10.1007/s00382-016-3030-x>
- Committee to Review the Edwards Aquifer Habitat Conservation Plan. (2018). Phase 3, water science and technology board, Division on Earth and Life Studies, and National Academies of Sciences, Engineering, and Medicine. In *Review of the Edwards Aquifer Habitat Conservation Plan: Report 3*. 25200. National Academies Press. <https://doi.org/10.17226/25200>
- Condon, L. E., Atchley, A. L., & Maxwell, R. M. (2020). Evapotranspiration depletes groundwater under warming over the contiguous United States. *Nature Communications*, 11(1), 873. <https://doi.org/10.1038/s41467-020-14688-0>

## Acknowledgments

We thank the anonymous reviewers of this article for their comments and critiques of this article. This research was supported by the Edwards Aquifer Authority, USA (Project # 22-016-AMS) and the United States Geological Survey's South Central Climate Adaptation Science Center (G21AC10751). Any opinion, findings, conclusions, and recommendations expressed in the publication are solely those of the authors. The computing for this project was performed at the OU Supercomputing Center for Education and Research (OSCAR) at the University of Oklahoma. OSCAR Executive Director Henry Neeman and OSCAR Senior Systems Analyst David Atkin provided valuable technical expertise.



- Costantini, M., Colin, J., & Decharme, B. (2023). Projected climate-driven changes of water table depth in the world's major groundwater basins. *Earth's Future*, 11(3), e2022EF003068. <https://doi.org/10.1029/2022EF003068>
- Crosbie, R. S., Dawes, W. R., Charles, S. P., Mpelasoka, F. S., Aryal, S., Barron, O., & Summerell, G. K. (2011). Differences in future recharge estimates due to GCMs, downscaling methods and hydrological models: Future recharge estimates. *Geophysical Research Letters*, 38(11). <https://doi.org/10.1029/2011GL047657>
- Devitt, T. J., Wright, A. M., Cannatella, D. C., & Hillis, D. M. (2019). Species delimitation in endangered groundwater salamanders: Implications for aquifer management and biodiversity conservation. *Proceedings of the National Academy of Sciences*, 116(7), 2624–2633. <https://doi.org/10.1073/pnas.1815014116>
- Dixon, K. W., Wootten, A. M., Nath, M. J., Lanzante, J., Adams-Smith, D. J., Whitlock, C. F., et al. (2020). *South central climate projections evaluation project (C-PrEP)*. South Central Climate Adaptation Science Center. <https://doi.org/10.21429/12gk-dh47>
- ESGF User Support Working Team. (2019). Earth system grid federation: Federated nodes [website] Retrieved from <https://aims2.llnl.gov/search/cmip6/>
- Eyring, V., Bony, S., Meehl, G. A., Senior, C. A., Stevens, B., Stouffer, R. J., & Taylor, K. E. (2016). Overview of the coupled model Inter-comparison project Phase 6 (CMIP6) experimental design and organization. *Geoscientific Model Development*, 9(5), 1937–1958. <https://doi.org/10.5194/gmd-9-1937-2016>
- Famiglietti, J. S. (2014). The global groundwater crisis. *Nature Climate Change*, 4(11), 945–948. <https://doi.org/10.1038/nclimate2425>
- Ferguson, G., & Gleeson, T. (2012). Vulnerability of coastal aquifers to groundwater use and climate change. *Nature Climate Change*, 2(5), 342–345. <https://doi.org/10.1038/nclimate1413>
- Franklin, J., Davis, F. W., Ikegami, M., Syphard, A. D., Flint, L. E., Flint, A. L., & Hannah, L. (2013). Modeling plant species distributions under future climates: How fine scale do climate projections need to be? *Global Change Biology*, 19(2), 473–483. <https://doi.org/10.1111/gcb.12051>
- Fu, Z., Xie, Y., Zhang, Y., Jiang, X., Guo, H., & Wang, S. (2022). Water resource availability assessment through hydrological simulation under climate change in the Huangshui watershed of the Qinghai–Tibet plateau. *Frontiers in Earth Science*, 9, 755119. <https://doi.org/10.3389/feart.2021.755119>
- Giordano, M. (2009). Global groundwater? Issues and solutions. *Annual Review of Environment and Resources*, 34(1), 153–178. <https://doi.org/10.1146/annurev.enviro.030308.100251>
- Giuntoli, I., Villarini, G., Prudhomme, C., & Hannah, D. M. (2018). Uncertainties in projected runoff over the conterminous United States. *Climatic Change*, 150(3–4), 149–162. <https://doi.org/10.1007/s10584-018-2280-5>
- Gordu, F., & Nachabe, M. H. (2023). Inferences of groundwater response to projected hydroclimatic changes in North Florida. *Journal of Hydrologic Engineering*, 28(4), 04023001. <https://doi.org/10.1061/JHYEFF.HEENG-5827>
- Hausfather, Z., Marvel, K., Schmidt, G. A., Nielsen-Gammon, J. W., & Zelinka, M. (2022). Climate simulations: Recognize the ‘hot model’ problem. *Nature*, 605(7908), 26–29. <https://doi.org/10.1038/d41586-022-01192-2>
- Hawkins, E., & Sutton, R. (2009). The potential to narrow uncertainty in regional climate predictions. *Bulletin of the American Meteorological Society*, 90(8), 1095–1107. <https://doi.org/10.1175/2009BAMS2607.1>
- Hawkins, E., & Sutton, R. (2011). The potential to narrow uncertainty in projections of regional precipitation change. *Climate Dynamics*, 37(1), 407–418. <https://doi.org/10.1007/s00382-010-0810-6>
- Hayhoe, K., Stoner, A., Wuebbles, D. J., & Scott-Fleming, I. (2023). STAR-ESDM: A generalizable approach to generating high-resolution climate projections through signal decomposition. *Authorea Preprints*. <https://doi.org/10.22541/essoar.169462036.65393270/v1>
- Jagannathan, K., Buddhavarapu, S., Ullrich, P. A., & Jones, A. D. (2023). Typologies of actionable climate information and its use. *Global Environmental Change*, 82, 102732. <https://doi.org/10.1016/j.gloenvcha.2023.102732>
- Jagannathan, K., Jones, A. D., & Kerr, A. C. (2020). Implications of climate model selection for projections of decision-relevant metrics: A case study of chill hours in California. *Climate Services*, 18, 100154. <https://doi.org/10.1016/j.cliser.2020.100154>
- Jagannathan, K., Jones, A. D., & Ray, I. (2021). The making of a metric: Co-producing decision-relevant climate science. *Bulletin of the American Meteorological Society*, 102(8), E1579–E1590. <https://doi.org/10.1175/BAMS-D-19-0296.1>
- Jaramillo, P., & Nazemi, A. (2018). Assessing urban water security under changing climate: Challenges and ways forward. *Sustainable Cities and Society*, 41, 907–918. <https://doi.org/10.1016/j.scs.2017.04.005>
- Keller, A. A., Garner, K. L., Rao, N., Knipping, E., & Thomas, J. (2022). Downscaling approaches of climate change projections for watershed modeling: Review of theoretical and practical considerations. *PLOS Water*, 1(9), e0000046. <https://doi.org/10.1371/journal.pwat.0000046>
- Kloesel, K., Bartush, B., Banner, J., Brown, D., Lemery, J., Lin, X., et al. (2018). Chapter 23: Southern Great Plains. Impacts, risks, and adaptation in the United States: The fourth national climate assessment, volume II. *U.S. Global Change Research Program*. <https://doi.org/10.7930/NCA4.2018.CH23>
- Krysanova, V., Donnelly, C., Gelfan, A., Gerten, D., Arheimer, B., Hattermann, F., & Kundzewicz, Z. W. (2018). How the performance of hydrological models relates to credibility of projections under climate change. *Hydrological Sciences Journal*, 63(5), 696–720. <https://doi.org/10.1080/02626667.2018.1446214>
- Lafferty, D. C., & Srivier, R. L. (2023). Downscaling and bias-correction contribute considerable uncertainty to local climate projections in CMIP6. *Npj Climate and Atmospheric Science*, 6(1), 158. <https://doi.org/10.1038/s41612-023-00486-0>
- Lall, U., Johnson, T., Colohan, P., Aghakouchak, A., Arumugam, S., Brown, C., et al. (2018). Chapter 3: Water. Impacts, risks, and adaptation in the United States: The fourth national climate assessment, volume II. *U.S. Global Change Research Program*. <https://doi.org/10.7930/NCA4.2018.CH3>
- Lanzante, J. R., Dixon, K. W., Adams-Smith, D., Nath, M. J., & Whitlock, C. E. (2021). Evaluation of some distributional downscaling methods as applied to daily precipitation with an eye towards extremes. *International Journal of Climatology*, 41(5), 3186–3202. <https://doi.org/10.1002/joc.7013>
- Lanzante, J. R., Nath, M. J., Whitlock, C. E., Dixon, K. W., & Adams-Smith, D. (2019). Evaluation and improvement of tail behaviour in the cumulative distribution function transform downscaling method. *International Journal of Climatology*, 39(4), 2449–2460. <https://doi.org/10.1002/joc.5964>
- Li, H., Sheffield, J., & Wood, E. F. (2010). Bias correction of monthly precipitation and temperature fields from Intergovernmental Panel on Climate Change AR4 models using equidistant quantile matching. *Journal of Geophysical Research*, 115(D10). <https://doi.org/10.1029/2009JD012882>
- Lindgren, R. J., Dutton, A. R., Hovorka, S. D., Worthington, S. R. H., & Painter, S. (2004). Conceptualization and simulation of the Edwards aquifer, san Antonio region, Texas. Report No. 2004–5277. *Scientific Investigations Report*. <https://doi.org/10.3133/sir20045277>
- Loáiciga, H. A. (2009). Long-term climatic change and sustainable ground water resources management. *Environmental Research Letters*, 4(3), 035004. <https://doi.org/10.1088/1748-9326/4/3/035004>



- Loaiciga, H. A., Maidment, D. R., & Valdes, J. B. (2000). Climate-change impacts in a regional karst aquifer, Texas, USA. *Journal of Hydrology*, 227(1–4), 173–194. [https://doi.org/10.1016/S0022-1694\(99\)00179-1](https://doi.org/10.1016/S0022-1694(99)00179-1)
- Maraun, D. (2023). The challenge of providing information about regional climate change. In S. Hummel, P. Assinger, C. Bauer, T. Brudermann, A. Jany, M. Jury, et al. (Eds.), *Shaping tomorrow today – SDGs from multiple perspectives* (pp. 15–46). Springer Fachmedien Wiesbaden. [https://doi.org/10.1007/978-3-658-38319-0\\_2](https://doi.org/10.1007/978-3-658-38319-0_2)
- Margat, J., & Gun, J. V. D. (2013). *Groundwater around the world* (0 ed.). CRC Press. <https://doi.org/10.1201/b13977>
- Marvel, K., Su, W., Delgado, R., Aarons, S., Chatterjee, A., Garcia, M. E., et al. (2023). Climate trends. In A. R. Crimmins, C. W. Avery, D. R. Easterling, K. E. Kunkel, B. C. Stewart, & T. K. Maycock (Eds.), *Fifth National Climate Assessment*. U.S. Global Change Research Program. <https://doi.org/10.7930/NCA5.2023.CH2>
- McCabe, G. J., & Wolock, D. M. (2016). Variability and trends in runoff efficiency in the conterminous United States. *JAWRA Journal of the American Water Resources Association*, 52(5), 1046–1055. <https://doi.org/10.1111/1752-1688.12431>
- McSweeney, C. F., Jones, R. G., Lee, R. W., & Rowell, D. P. (2015). Selecting CMIP5 GCMs for downscaling over multiple regions. *Climate Dynamics*, 44(11–12), 3237–3260. <https://doi.org/10.1007/s00382-014-2418-8>
- Neves, G. L., Barbosa, M. A. G. A., Anjinho, P. D. S., Guimarães, T. T., Das Virgens Filho, J. S., & Mauad, F. F. (2020). Evaluation of the impacts of climate change on streamflow through hydrological simulation and under downscaling scenarios: Case study in a watershed in southeastern Brazil. *Environmental Monitoring and Assessment*, 192(11), 707. <https://doi.org/10.1007/s10661-020-08671-x>
- O'Neill, B. C., Tebaldi, C., Van Vuuren, D. P., Eyring, V., Friedlingstein, P., Hurtt, G., et al. (2016). The scenario model Intercomparison project (ScenarioMIP) for CMIP6. *Geoscientific Model Development*, 9(9), 3461–3482. <https://doi.org/10.5194/gmd-9-3461-2016>
- Parding, K. M., Dobler, A., McSweeney, C. F., Landgren, O. A., Benestad, R., Erlandsen, H. B., et al. (2020). GCMeval – An interactive tool for evaluation and selection of climate model ensembles. *Climate Services*, 18, 100167. <https://doi.org/10.1016/j.cliser.2020.100167>
- Pierce, D. W., Cayan, D. R., Feldman, D. R., & Risser, M. D. (2023). Future increases in North American extreme precipitation in CMIP6 downscaled with LOCA. *Journal of Hydrometeorology*, 24(5), 951–975. <https://doi.org/10.1175/JHM-D-22-0194.1>
- Pierce, D. W., Cayan, D. R., Maurer, E. P., Abatzoglou, J. T., & Hegewisch, K. C. (2015). Improved bias correction techniques for hydrological simulations of climate change. *Journal of Hydrometeorology*, 16(6), 2421–2442. <https://doi.org/10.1175/JHM-D-14-0236.1>
- Piotrowski, A. P., Osuch, M., & Napiorkowski, J. J. (2021). Influence of the choice of stream temperature model on the projections of water temperature in rivers. *Journal of Hydrology*, 601, 126629. <https://doi.org/10.1016/j.jhydrol.2021.126629>
- Pourmokhtarian, A., Driscoll, C. T., Campbell, J. L., Hayhoe, K., & Stoner, A. M. K. (2016). The effects of climate downscaling technique and observational dataset on modeled ecological responses. *Ecological Applications*, 26(5), 1321–1337. <https://doi.org/10.1890/15-0745>
- Rahimpour Asenjan, M., Brissette, F., Martel, J.-L., & Arsenault, R. (2023). The dilemma of including “hot” models in climate impact studies: A hydrological study (preprint). *Hydrometeorology/Modelling approaches*. <https://doi.org/10.5194/hess-2023-47>
- RECON Environmental Inc., Hicks & Company, Zara Environmental LLC & BIO-WEST. (2012). Edwards aquifer recovery implementation program habitat conservation plan. Retrieved from <https://www.edwardsaquifer.org/wp-content/uploads/2022/07/Edwards-Aquifer-Recovery-Implementation-Program-Nov-2021.pdf>
- Riahi, K., Grübler, A., & Nakicenovic, N. (2007). Scenarios of long-term socio-economic and environmental development under climate stabilization. *Technological Forecasting and Social Change*, 74(7), 887–935. <https://doi.org/10.1016/j.techfore.2006.05.026>
- Rosegrant, M. W., Ringler, C., & Zhu, T. (2009). Water for agriculture: Maintaining food security under growing scarcity. *Annual Review of Environment and Resources*, 34(1), 205–222. <https://doi.org/10.1146/annurev.enviro.030308.090351>
- Ross, A. C., & Najjar, R. G. (2019). Evaluation of methods for selecting climate models to simulate future hydrological change. *Climatic Change*, 157(3–4), 407–428. <https://doi.org/10.1007/s10584-019-02512-8>
- Rummukainen, M. (2010). State-of-the-art with regional climate models. *Wiley Interdisciplinary Reviews-Climate Change*, 1(1), 82–96. <https://doi.org/10.1002/wcc.008>
- Rummukainen, M. (2016). Added value in regional climate modeling. *Wiley Interdisciplinary Reviews: Climate Change*, 7(1), 145–159. <https://doi.org/10.1002/wcc.378>
- Russo, T. A., & Lall, U. (2017). Depletion and response of deep groundwater to climate-induced pumping variability. *Nature Geoscience*, 10(2), 105–108. <https://doi.org/10.1038/ngeo2883>
- Sanderson, B. M., Wehner, M., & Knutti, R. (2017). Skill and independence weighting for multi-model assessments. *Geoscientific Model Development*, 10(6), 2379–2395. <https://doi.org/10.5194/gmd-10-2379-2017>
- Schindel, G. M. (2019). Genesis of the Edwards (Balcones fault zone) aquifer. In J. M. Sharp, R. T. Green, & G. M. Schindel (Eds.), *The Edwards Aquifer: The Past, Present, and Future of a Vital Water Resource*. Geological Society of America. [https://doi.org/10.1130/2019.1215\(02](https://doi.org/10.1130/2019.1215(02)
- Scibek, J., & Allen, D. M. (2006). Modeled impacts of predicted climate change on recharge and groundwater levels: Impacts of climate change on recharge. *Water Resources Research*, 42(11). <https://doi.org/10.1029/2005WR004742>
- Shaabani, M. K., Abedi-Koupai, J., Eslamian, S. S., & Gohari, A. (2023). Simulation of the effects of climate change and reduce irrigation requirements on groundwater recharge using SWAT and MODFLOW models. *Modeling Earth Systems and Environment*, 9(2), 1681–1693. <https://doi.org/10.1007/s40808-022-01580-7>
- Siebert, S., Burke, J., Faures, J. M., Frenken, K., Hoogeveen, J., Döll, P., & Portmann, F. T. (2010). Groundwater use for irrigation – A global inventory. *Hydrology and Earth System Sciences*, 14(10), 1863–1880. <https://doi.org/10.5194/hess-14-1863-2010>
- Sun, A. Y., Bonigovanni, T., Caldwell, T. G., & Young, M. H. (2020). Quantifying diffuse recharge at Camp Bullis, TX: Integrating soil water, evapotranspiration, and remote sensing. 2020 Final Report, Submitted to the Edwards Aquifer Authority.
- Tabari, H., De Troch, R., Giot, O., Hamdi, R., Termonia, P., Saeed, S., et al. (2016). Local impact analysis of climate change on precipitation extremes: Are high-resolution climate models needed for realistic simulations? *Hydrology and Earth System Sciences Discussions*, 2016(March), 1–21. <https://doi.org/10.5194/hess-2016-106>
- Thornton, M. M., Shrestha, R., Wei, Y., Thornton, P. E., Kao, S.-C., & Wilson, B. E. (2022). *Daymet: Daily surface weather data on a 1-km grid for North America, version 4 R1*. ORNL Distributed Active Archive Center. <https://doi.org/10.3334/ORNLDAA/2129>
- Trudel, M., Doucet-Généreux, P.-L., & Leconte, R. (2017). Assessing River low-flow uncertainties related to hydrological model calibration and structure under climate change conditions. *Climate*, 5(1), 19. <https://doi.org/10.3390/cli5010019>
- U.S. Fish and Wildlife Service. (2015). Fish and Wildlife service-endangered species act - incidental Take Permit amendment. TE63663A-1. [https://www.edwardsaquifer.org/wp-content/uploads/2019/02/USFWS\\_response\\_to\\_Refugia\\_amendment.pdf](https://www.edwardsaquifer.org/wp-content/uploads/2019/02/USFWS_response_to_Refugia_amendment.pdf)
- van Vuuren, D. P., Edmonds, J., Kainuma, M., Riahi, K., Thomson, A., Hibbard, K., et al. (2011). The representative concentration pathways: An overview. *Climatic Change*, 109(1), 5–31. <https://doi.org/10.1007/s10584-011-0148-z>
- Wootten, A., Terando, A., Reich, B. J., Boyles, R. P., & Semazzi, F. (2017). Characterizing sources of uncertainty from global climate models and downscaling techniques. *Journal of Applied Meteorology and Climatology*, 56(12), 3245–3262. <https://doi.org/10.1175/JAMC-D-17-0087.1>
- Wootten, A. M. (2024a). Climate analysis and evaluation tools v 1.0 (research) [Code]. *Zenodo*. <https://doi.org/10.5281/zenodo.12775391>

- Wootten, A. M. (2024b). Ensemble subset selection Algorithm v 1.0 (research) [Code]. *Zenodo*. <https://doi.org/10.5281/zenodo.12775364>
- Wootten, A. M., Başağaoğlu, H., & Bertetti, F. P. (2024). Downscaled climate projections for the Edwards aquifer region (EAR) using CMIP5 for the years 2006-2100 and CMIP6 for the years 2015-2100 [Dataset]. *U.S. Geological Survey Data release*. <https://doi.org/10.5066/P13NMKWU>
- Wootten, A. M., Dixon, K. W., Adams-Smith, D. J., & McPherson, R. A. (2020). Statistically downscaled precipitation sensitivity to gridded observation data and downscaling technique. *International Journal of Climatology*, 41(June), 1–22. <https://doi.org/10.1002/joc.6716>
- Wootten, A. M., Martin, E., Randklev, C. R., & Smith, R. (2023). Projected changes to streamflow and stream temperature in central Texas: How much will the river flow? *Earth Interactions*, 27(1), 220021. <https://doi.org/10.1175/EI-D-22-0021.1>
- Wu, W.-Y., Lo, M.-H., Wada, Y., Famiglietti, J. S., Reager, J. T., Yeh, P. J.-F., et al. (2020). Divergent effects of climate change on future groundwater availability in key mid-latitude aquifers. *Nature Communications*, 11(1), 3710. <https://doi.org/10.1038/s41467-020-17581-y>